BULLETIN OF THE POLISH ACADEMY OF SCIENCES
TECHNICAL SCIENCES, Vol. 67, No. 4, 2019
DOI: 10.24425/bpasts.2019.130188

Analysis and investigations of inductive power transfer (IPT) systems in terms of efficiency and magnetic field distribution properties

R.M. MIŚKIEWICZ*, P. ANCZEWSKI, and A.J. MORADEWICZ

Łukasiewicz Research Network – Electrotechnical Institute, Pożaryskiego St. 28, 04-703 Warsaw, Poland

Abstract. The problems connected to developing inductive power transfer IPT systems in aspects of high efficiency and suppression of electromagnetic field (EMF) emission are discussed. It is shown how important it is to compensate for large leakage impedance of IPT coils (air transformer) to improve efficiency of high power transfer. Such compensation circuits operating with resonant frequencies at soft switching conditions additionally allow for reduction of switching losses in power semiconductor devices of converters. The consideration has been illustrated and verified by experimental results measured on two different test stands (50 kW with planar coils and with two 12 kW receiver coils) built in a laboratory of the Łukasiewicz Research Network – Electrotechnical Institute.

Key words: contactless energy transfer, inductive power transfer, resonant compensation circuits, electromagnetic field distribution.

1. Introduction

Recently, a large number of technologies for contactless energy transfer CET (also called wireless power transfer WPT) systems have been established. Generally, the CET systems are based on various power transfer media [1–3]: sound (ultrasound), light (laser), capacitive and inductive coupling. In the case of inductive CET systems, two types are currently distinguished: inductive power transfer – IPT and strongly coupled magnetic resonance – SCMR systems [2–4]. The IPT forms a group of systems operating at high power (1–100 kW and more) with air gap up to 30–40 cm and frequencies up to 100 kHz. In contrast, the SCMR is a group operating at low power 1–1000 W and much larger distance, even up to a few meters and high frequencies in the order of MHz-GHz [5].

In this article, we refer to IPT systems following this nomenclature. IPT are increasingly used in everyday devices as an alternative way of powering various devices. An example of such solutions is the power supply of mobile phones, tablets, medical etc [6–8]. However, it is also observing individual applications that supply energy to devices requiring much higher power level, such as: electric vehicles [9–21], wheeled and rail, and ships [22].

Contrarily to conventional transformers, in IPT systems the coupling between primary and secondary coils is low or very low. Therefore, main factor limiting the energy transfer are voltage drops on the leakage inductances of the winding, which increase as the magnetic coupling factor k decreases. The solution of this problem is the use of resonant compensation circuits [1, 2, 21, 23]. Regardless of the complexity of the systems for a given application, in order to analyze it, the components of IPT are brought to the basic structure (Fig. 1). The basic system consists of a transmitting resonant converter, which converts voltage or direct current into a rectangular waveform, a receiving converter that converts high frequency alternating signals into current and DC voltage as well as a resonant compensation circuit. The compensation circuit includes primary and secondary coils, resonant capacitors and/or additional LC elements. The choice of the compensation circuit and its parameters depends on such expected IPT system properties as: type of supply converter (diode or transistor active rectifier) transmitted power level and distance, and what type of receiver should be powered. Depending on the needs of the designed system, the role of the transmitting and receiving converter can be interchangeable; this takes place in systems with bi-directional energy flow [18, 23, 25]. Additional converters are systems which, on the power supply side, provide reductions of higher harmonics of the grid current and unity power factor operation. While on the receiver side it is a converter that adjusts the voltage or current to the receiver requirements, e.g. adapted to the connected battery bank.

The article presents an analysis and design aspects of IPT systems achieving high efficiency in power range up to 50 kW. Also, what impact the designed system will have on the external environment as: impact on living organisms and electronic devices that may be found nearby. Therefore, appropriate method of suppression of electromagnetic field (EMF) emission is necessary. The consideration has been illustrated and verified by FEM (Finite Element Method) simulation and experimental results measured on two different high efficiency IPT test stands (12 kW and 50 kW) built in laboratory of The Łukasiewicz Research Network – Electrotechnical Institute. Presented results have shown that both variants of discussed IPT systems fulfil the General Public Electromagnetic Radiation Standard According to the International Commission of Non-Ionized Radiation Protection – (ICNIRP) 2010 [39].

*e-mail: r.miskiewicz@iel.waw.pl

Manuscript submitted 2019-05-22, revised 2019-07-02, initially accepted for publication 2019-07-22, published in August 2019

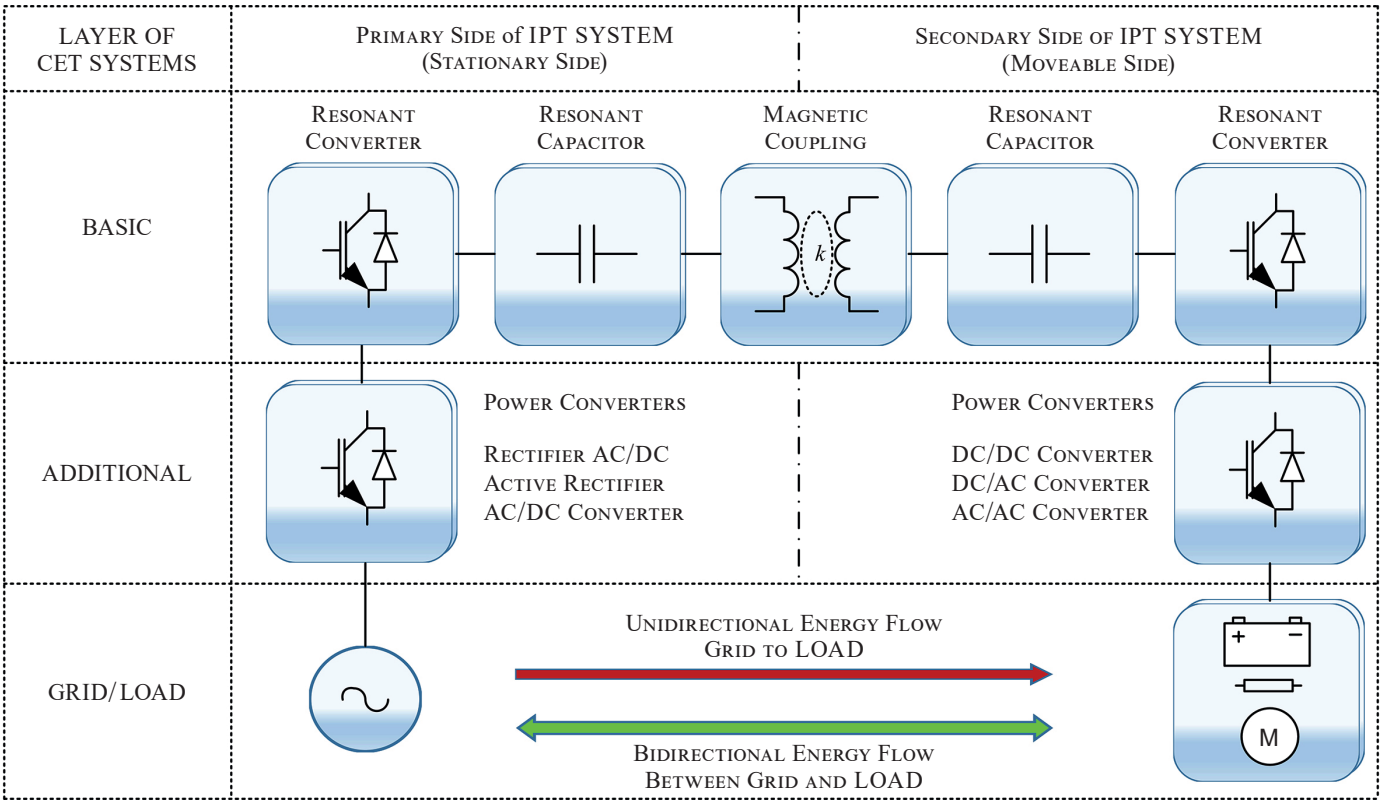

Fig. 1. Functional block diagram of inductive IPT system

2. Resonant compensation circuits

2.1. Problem of low coupling factor. The basic problem in inductive coupling systems are voltage drops caused by the leakage inductances of primary and secondary coils, which increases as the magnetic coupling factor k decreases. This is illustrated by the equivalent circuit in Fig. 2 and is described by complex transfer functions (4), (5), (6), where:

$$k = \frac{M}{\sqrt{L_p L_s}} \tag{1}$$

$$L_p = L_{rp} + M = L_{rp} + k\sqrt{L_p L_s} \tag{2}$$

$$L_s = L_{rs} + M = L_{rs} + k\sqrt{L_p L_s}\,. \tag{3}$$

$$\begin{aligned} G_v(s) = \frac{U_s(s)}{U_p(s)} &= \frac{sR_oM}{s^2\left(L_{rp}L_{rs} + ML_{rs} + ML_{rp}\right) + s\left(R_p\left(L_{rs}+M\right) + \left(R_s+R_o\right)\left(L_{rp}+M\right)\right) + R_pR_s + R_pR_o} = \\ &= \frac{sR_oM}{s^2L_pL_s\left(1-k^2\right) + sR_pR_s\left(R_pL_s + \left(R_s+R_o\right)L_p\right) + R_pR_s + R_pR_o} \end{aligned} \tag{4}$$

$$G_i(s) = \frac{I_s(s)}{I_p(s)} = \frac{sM}{s\left(L_{rs}+M\right) + R_s + R_o} = \frac{sM}{sL_s + R_s + R_o} \tag{5}$$

$$\begin{aligned} Z_{we}(s) = \frac{U_p(s)}{I_p(s)} &= \frac{s^2\left(L_{rp}L_{rs} + ML_{rs} + ML_{rp}\right) + s\left(R_p\left(L_{rs}+M\right) + \left(R_s+R_o\right)\left(L_{rp}+M\right)\right) + R_pR_s + R_pR_o}{s\left(L_{rs}+M\right) + R_s + R_o} = \\ &= \frac{s^2L_pL_s\left(1-k^2\right) + s\left(R_pL_s + \left(R_s+R_o\right)L_p\right) + R_pR_s + R_pR_o}{sL_s + R_s + R_o} \end{aligned} \tag{6}$$

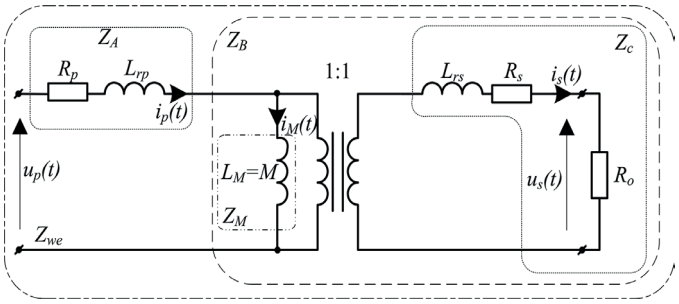

Fig. 2. Transformer equivalent circuit of the IPT system

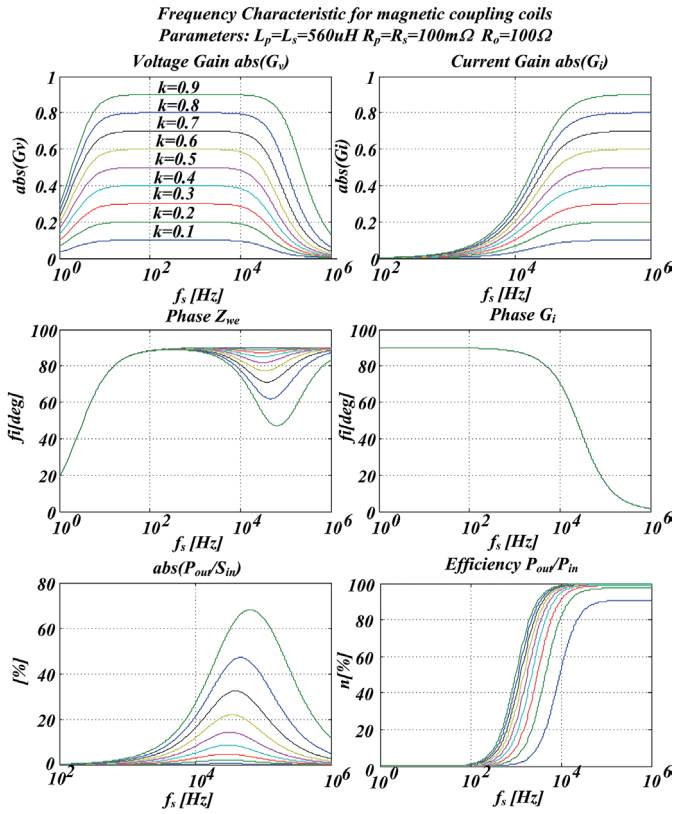

Fig. 3. Frequency characteristics of magnetic coupled coils without compensation circuit

These equations can be illustrated by frequency characteristics shown in Fig. 3. As it can be seen, for symmetrical windings with constant self inductance $L_p = L_s$, and load resistance R_o, the voltage gain Gv depends on k, especially for small resistance of windings R_p, R_s.

For different self inductances $L_p \neq L_s$, the voltage gain is proportional to turns ratio $Gv = N\,k$ [23]. The efficiency of such a system for low and medium frequencies is low, but as the current gain Gi increases, the efficiency also increases and is directly dependent on the circuit resistance $(R_p + R_s)$. Changing of the load resistance R_o causes changes of frequency bandwidth [27].

2.2. Influence of the compensation circuit. To enable high-efficiency energy transfer regardless of the magnetic coupling factor k value (1), various compensation circuits with capacitors connected in series or parallel are used to cancel large leakage inductance of coupled coils [1, 21, 23]. All compensation circuits described in the literature have their advantages and disadvantages, depending on the place of application and the type of receiver being fed (see Table 1) [18, 26, 27, 29, 30]. Among the main requirements are: high efficiency, maximize transferred power at minimum reactive power taken from power supply, tolerance to coils misalignments. Often the basic criterion for the compensation circuit selection is operation in the widest range of changes of the magnetic coupling factor k (if this takes place in the designed system) and changes in the system load R_o. Two topologies that meet these criteria can be distinguished: S-S series-series (Fig. 4) and modified LCL [23]. However, the

Table 1
Comparison of different compensation circuits

Name of resonant circuit	Input character	Output character	High efficiency Bi-directional Energy flow	Resonant frequency
Series – Parallel (S – P)	Voltage	Current	YES	Two resonant frequencies. One depend on k and R_o
Parallel – Series (P – S)	Current	Voltage	YES	Two resonant frequencies. One depend on k and R_o
Series – Series (S – S)	Voltage	Voltage	YES	Two resonant frequencies. Independent of k and R_o
Parallel – Parallel (P – P)	Current	Current	YES	Depend on k and R_o
Series – LCL (S – LCL)	Voltage	Voltage	YES	Three resonant frequency one independent on k and R_o, two subsidiaries
LCL – Series (LCL – S)	Voltage	Voltage	YES	Four resonances frequencies one independent on k and R_o, three subsidiaries

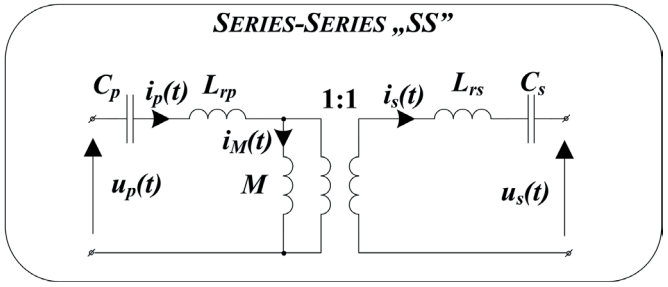

Fig. 4. Topology of S-S compensation circuit

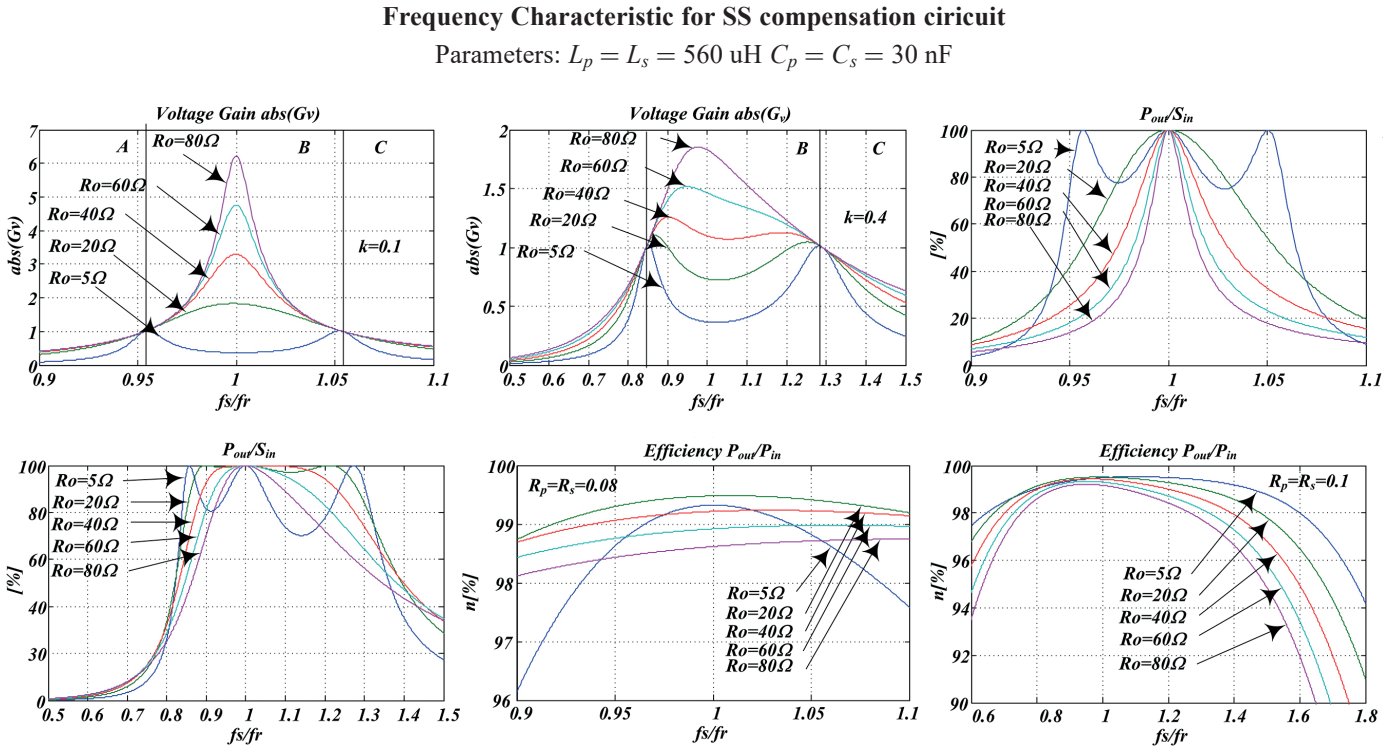

Fig. 5. Frequency characteristics of magnetic coupled coils with S-S compensation circuit for magnetic coupling factor $k = 0.1$ and $k = 0.4$ and load resistance R_o as parameter

most popular compensation circuit used in IPT systems is the series-series (S-S), because it is simpler in design and control compared to LCL circuits.

The frequency characteristics of the magnetic coupled coils with S-S compensation circuit, are shown in Fig. 5. (The detailed derivation of transfer functions can be found in [23]). Based on these characteristics, three zones of voltage amplification A, B, C can be distinguished. In zone A, the system is characterized by the capacitive character of the circuit and in the zone B and C by the inductive character. The voltage gain decreases as frequency changes and depends on the load resistance value R_o and the magnetic coupling factor k. In the zone B the system has the ability to significantly lowering or raise voltage; the lower is resistance R_o the lower the voltage gain of the system. Thus, among the main advantages of S-S circuit are: operation in a wide range of the coupling factor k changes without having to change parameters of the compensation capacitors, because their selection is independent of k and R_o:

$$C_s = \frac{1}{\omega_{r1}^2 L_s} \quad \text{and} \quad C_s = \frac{1}{\omega_{r1}^2 L_s}, \tag{7}$$

symmetrical structure and possibility of bi-directional energy flow, flexibility in parameter selection for both constant and variable operation frequency to obtain the required output power at minimum windings current, low sensitivity to coils misalignment [21, 23, 27].

3. Suppression of EMF emission

Contactless energy transfer in IPT devices are based on magnetically coupled coils generating electromagnetic field (EMF) radiation. Therefore, the basic problem when designing and apply IPT is question: is it safe for human health? Although researchers argue that IPT devices are much safer than massively used smart phones [9], methods for attenuating and compensating EMF emissions are still being developed to ensure compliance with international emission standards particularly for higher power IPT. There are a number of standards regarding limits of EMF emission. In addition to general like IEEE: "*C95.1–2005-IEEE Standard for Safety Levels with Respect to Human Frequency, Radio Frequency Electromagnetic Fields, 3 kHz to 300 GHz*" [38] and ICNIRP: "*Guidelines for limiting exposure to time-varying electric and magnetic fields (1 Hz to 100 kHz)*" [39], there are also standards addressed to specific IPT devices, e.g. established for EV – battery chargers by SAE [40] as well as by IEC [41]. Generally, the leakage EMF of IPT must comply with ICNIRP 2010 standards (as also recommended in SAE J2954/1) while the IEEE offers more insights into physiological effects such as nerve excitation (<100 kHz) and tissue heating (>100 kHz).

According to the ICNIRP 2010 guideline, the magnetic field limit for 3 kHz to 100 kHz is:

- 27 μT_{rms} for general-public exposure,
- 100 μT_{rms} for occupational exposure,
- 15 μT_{rms} for areas where there may be people with an implanted pacemaker.

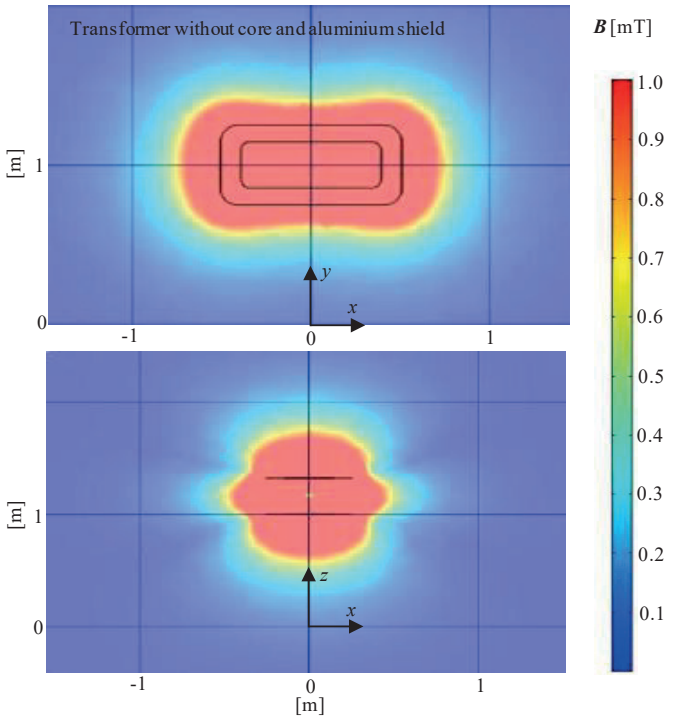

Fig. 6. FEM simulation of magnetic field distribution for coil without core; current 60 Arms, air gap (distance between coils) 30 cm and frequency 30 kHz. Scale of magnetic field induction in mTrms. a) view in xy-axis, b) view in zy-axis

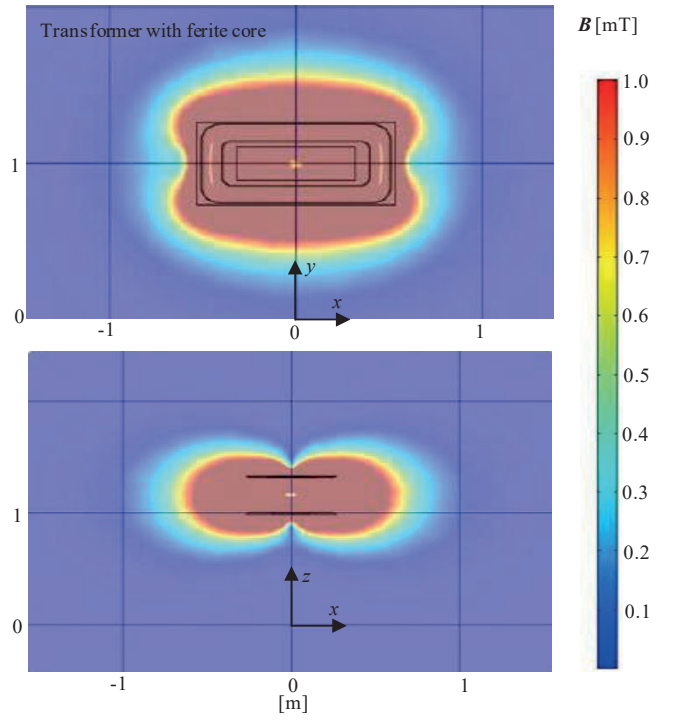

Fig. 7. FEM simulation of magnetic field distribution for coils with ferrite core; current 60 Arms, air gap (distance between coils) 30 cm and frequency 30 kHz. Scale of magnetic field induction in mTrms. a)view in xy-axis, b) view in zy-axis

To comply with these requirements, passive and active shielding methods are used . In passive methods typically aluminum or copper plate is placed on the backside of the ferrite and coils. The presence of shielding affects the performance of the system by reducing coil inductance and increasing losses which requires increasing of the compensation capacitance to keep resonance condition. The active shielding uses different placed additional coils to compensate for EMF emission. Both type of shielding can reduce the efficiency of a system by 1–3% [21, 37].

Three parameters: power level, coil geometry, and operating frequency play equally important roles in determining the leakage EMF. Therefore, as the first step of IPT coils design, is the FEM simulation. The example of such simulation for planar coils of Fig. 9 are shown in Fig. 6 and Fig. 7. It can be seen how the magnetic field induction B in z-y axis is reduced when ferrite core are used to suppress leakage flux (from ca 100 cm to 60 cm).

4. Experimental results

4.1. Description of laboratory test stands. The block diagram of the experimental test stands of the investigated IPT systems is shown in Fig. 8. The system is powered from a laboratory autotransformer connected to a three-phase active rectifier (AC-DC). Then, a single phase inverter (DC-AC) is used to supply the primary winding of the air transformer together with the leakage inductance compensation circuit (S-S). On the other side, the rectifier (AC-DC) and load are connected to the secondary side of the windings. In the developed system of IPT supply path, we can deal with the case of powering two systems at the same time as it is shown in the stand of Fig. 10.

Figure 9 and Fig. 10 show view of laboratory test stands with different coils configuration. In the first case (Fig. 9) is typical planar coils (air transformer) used e.g. in stationary charging stations. This stand has high self inductance (560 μH), nominal power 50 kW and works with frequency in the range

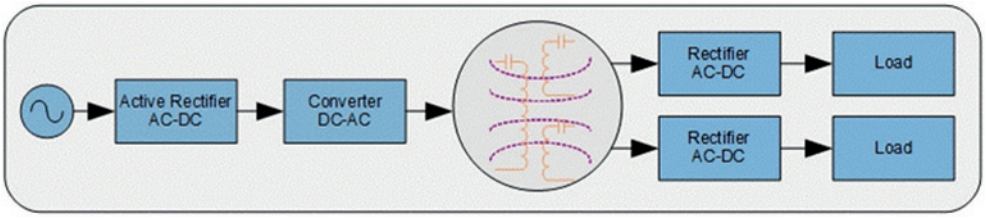

Fig. 8. Block diagram of the laboratory test stands of Fig. 9 and Fig. 10

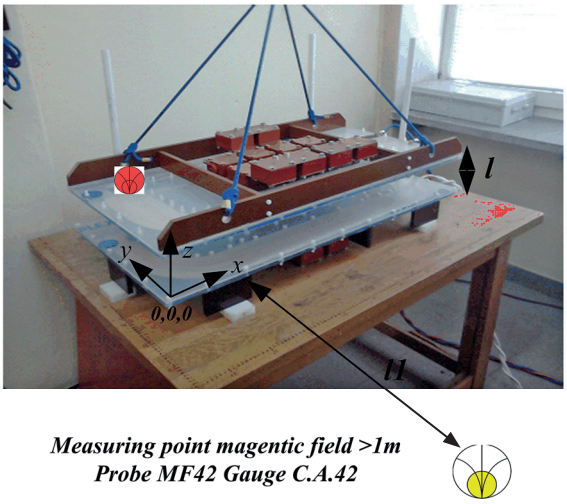

Fig. 9. View of 50 kW laboratory test stand (high primary self inductance) with measuring point of magnetic field distribution

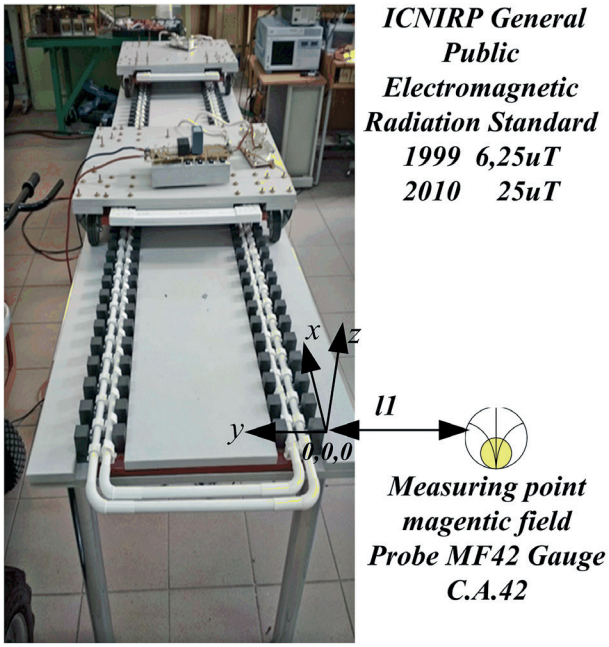

Fig. 10. View of 12 kW universal laboratory test stand (low primary self inductance) with measuring point of magnetic field distribution

Table 2
System parameters

Parameters	System in Fig. 9	System in Fig. 10
Power	25 kW	12 kW
IN/OUT voltage	600	600
Inductances Lp/Ls	560 uH/560 uH	40 uH/44 uH
Size of primary coil	1000×500 mm	3000×400 mm
Size of secondary coil	1000×500 mm	400×500 mm
Air-gap	50–300 mm	20 mm
Coupling factor k	0.54–0.13	0.259

of 40 to 60 kHz. The second test stand has coils configuration (Fig. 10) called sliding transformer [1] and can operate with two receivers. Self inductance of such configuration is small (40 μH) and inverter works with 85 kHz resonant frequency. In both Figures the point of measuring of magnetic field distribution and values of ICNIRP general public standards are shown.

4.2. Experimental results of IPT system (Fig. 9). The control possibilities depend strictly on the topology of applied resonance compensation circuit for voltage drops on leakage inductances of the IPT system. In the discussed S-S compensation circuit the most popular for adjustable output voltages or currents are methods [9, 15, 23, 25, 28, 32–34]:

- changing the operating frequency of the system (the phase angle between the input voltage and current) as follows: for high load power the operation at the resonant frequency f_{r2} and soft switching of converter; for low load power, the operation with a hard-switched converter [16, 18, 27].
- the use of the phenomenon of current suppression amplitude in a shorted resonant circuit – called integration method [32].
- operation at constant resonant frequency f_{r1} and adjustment of input voltage duty cycle (ang. Phase Shift Modulation – PSM) [8, 10, 12, 15, 25, 33, 34].

Generally, the constant-frequency PSM control method is recommended in the range of $k = 0.2 - 0.5$ where the voltage gain Gv as function of the load resistance R_o is the smallest. This offers better control possibilities. The frequency-variable method is recommended when IPT operates in a wide range changes of the coupling factor k.

Experimental oscillograms which illustrate operation of the S-S compensated IPT system under integration method (Fig. 11) and PSM control (Fig. 12). These oscillograms are measured on test stand of Fig. 9 in steady-state operation for resistive load and S-S circuit parameters: $L_p = L_s = 560$ μH, $C_p = C_s = 30$ nF, while Fig. 13 shows PSM operation for S-S

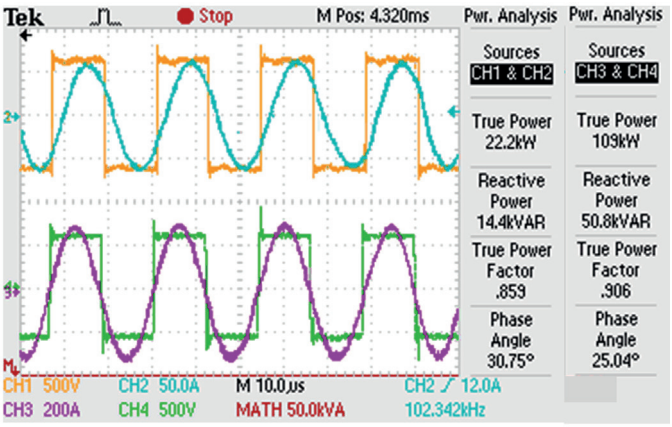

Fig. 11. Currents (i_p – CH1 scale: x1, i_s – CH3 scale: /5) and voltages (u_p – CH2 scale: x1, u_s – CH3 scale: x1) experimental waveforms in integration method controlled IPT system; magnetic coupling factor $k = 0.12$, air gap $l = 30$ cm, and a resistive load at the power $P_{in} = 22$ kW, operating frequency $f_{r2} = 41.9$ kHz, system efficiency $h = 92.5\%$

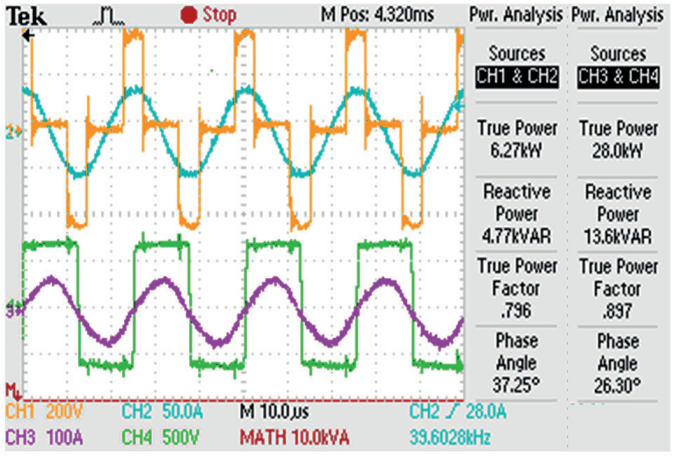

Fig. 12. Currents (i_p – CH1 scale: x1, i_s – CH3 scale /5) and voltages (u_p – CH2 scale: x1, u_s – CH3 scale: x1) experimental waveforms in PSM controlled IPT system; magnetic coupling factor $k = 0.12$, air gap $l = 30$ cm, and a resistive load at the power $P_{in} = 6.27$ kW, operating frequency $f_{r1} = 39.6$ kHz, system efficiency $h = 90\%$, $U_{dcin} = 400$ V

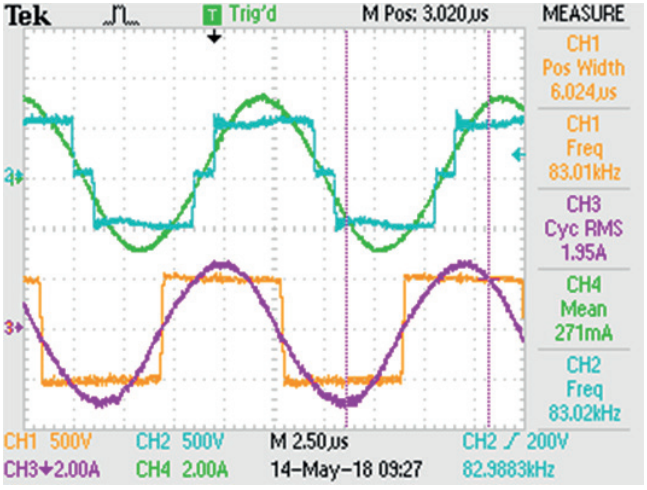

Fig. 13. Experimental results for S-S compensation circuit with constant frequency control (PSM method): $l = 19$ cm, $k = 0.12$, $P = 45.6$ kW $f_{r1} = 83$ kHz (i_p and i_s scale x50), (u_p – CH2 scale x1, u_s x1, 4 scale x1)

circuits parameters: $L_p = L_s = 80$ µH, $C_p = C_s = 40$ nF. These parameters are selected for resonant frequency ca 40 kHz and 85 kHz, respectively. The picture from the screen of Yokogawa (Fig. 14) presents an example of stationary parameters measured on the test stand of Fig. 9 operated under 45,6 kW input power with 92.6% efficiency.

4.3. Experimental results of IPT system (Fig. 10). The IPT system in Fig. 10 has two secondary coils allowing operation in various connection configurations between the power supply and the receiver (Table 3).

In the Table 3 "Two loads" means IPT systems have one primary coil and two independent secondary coils operated on

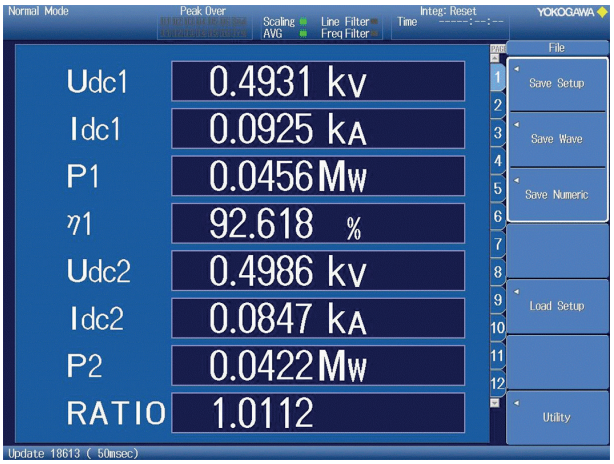

Fig. 14. Stationary parameters measured by Yokogawa on the test stand for transferred power P = 45,6 kW and efficiency 92.6%

resistive loads. The "Single load" means DC link converters of secondary coils are parallel connected and operate on common single resistive load.

If two independent different receivers are powered, a high efficiency between 92–97% can be achieved. In the case of the operation of two receivers on one common load, almost uniform power distribution between two secondary windings is possible [20]. In this case power of 12.75 kW under efficiency between 93–95% can be transferred. The third case examined (not shown in Table 3) is a complicated issue because one of the secondary coils acts as a power supply, and the second coil is a receiver.

Table 3
Results for the IPT system from Fig. 10

Operating mode	Part of IPT	Udc [V]	Idc [A]	Pdc [kW]	η [%]
Two loads Fig. 10	Primary	301	43	12.943	97
	Load 1	264	28	7.392	
	Load 2	313	16.4	5.133	
	Primary	301	16.7	5.026	92
	Load1	160	17	2.720	
	Load2	191	10	1.910	
Single load Fig. 10.	Primary	300	42.5	12.75	95
	Load1	234	24.0	5.616	
	Load2		28.0	6.552	
	Primary	300	17	5.1	93
	Load1	234	15.5	2.263	
	Load2		17.0	2.482	

where: Udc – source or load dc voltage, Idc – source or load dc current, Pdc – active power, η – efficiency

In such case, the power delivered to the second coil depends on the power delivered to the load.

4.4. Measurement of magnetic field distribution generated during IPT operation. The measurement of magnetic fields distribution has been performed using a magnetic field meter CAUVIN ARNOUX C.A. 42 and probes MF400 which measure the field strength of three axes. The magnetic field is expressed in rms value. In Fig. 9 measuring point in y axis was set 100cm from the edged coil and on the height of the primary winding z axis equal zero, x = 10 cm. This point shows limits of the ICNIRP 2010 General Public Electromagnetic Radiation Standard. In closer distains the emission intensity and induction field increase, and the highest values are achieved at edge of the coils and spaces between coils. The results of measurements for both test stands of Fig. 9 and Fig. 10 are shown in Table 4 and Table 5, respectively. The magnetic field increase with coil current (power) and decrease with distance of measuring point. In the test stand of Fig. 9, the magnetic field distribution in a distance of 100 cm for input power 22 kW, grows with distance between coils. For the worst case when the distance between coils is 40 cm, the magnetic field is 12 μT what is 48% of the ICNIRP general standards value 27 μT. Self inductance of coils configuration showed in Fig. 10 is low because of higher operating frequency 83 kHz. The emission of magnetic field in the distance 50 cm is 2.1 μT (Table 5) which is ca 8% of magnetic distribution value defined by the ICNIRP general standard. These results confirm a low level of magnetic field emission in the vicinity of the system.

Table 4
Results of magnectic field distribution for IPT stand in Fig. 9

Distance between coils [cm]	P_{in}	
	22 kW	6 kW
40	12,0 μT	6,5 μT
30	10,9 μT	5,5 μT
17	6,5 μT	4,2 μT
7	3,5 μT	2,0 μT

Table 5
Results of magnectic field distribution for IPT stand in Fig. 10

Distance of the measurement point [cm]	P_{in}	
	12 kW	3 kW
50	2,10 uT	0,90 uT
100	0,45 uT	0,29 uT
150	0,30 uT	0,13 uT

5. Conclusions

In this paper, problems linked to developing inductive power transfer IPT systems in aspects of high efficiency and suppressing of electromagnetic field EMF emission have been discussed. It was shown how the important losses caused by large leakage inductance of IPT coils (air transformer) can be compensated by use of resonant compensation circuits, particularly series – series (S-S) topology. Such resonant compensation circuits additionally allow for reducing switching losses in power semiconductor devices of converters. The consideration has been illustrated by FEM simulations and verified by experimental results measured on two different test stands (12 kW and 50 kW) built in a laboratory of the Łukasiewicz Research Network – Electrotechnical Institute. The performed measurements of magnetic field emission in the vicinity of 12 kW and 25 kW experimental IPT systems have confirmed a low level compliant with the ICNIRP 2010 General Public Electromagnetic Radiation Standard. However, in some special IPT applications, e.g. occupational, medical and electric vehicles, particularly higher power, more complicated active and passive shielding methods are necessary.

Acknowledgements. The project was financed by the National Science Centre NCN on the basis of decision no. DEC-2012/07/N/ST7/03487

References

[1] M.P. Kazmierkowski and A.J. Moradewicz, "Unplugged but Connected. Review of Contactless Energy Transfer Systems", *IEEE Industrial Electronics Magazine*, 6(4) 47–55 (2012).
[2] M.P. Kazmierkowski, R.M. Miśkiewicz, and A.J. Moradewicz, "Inductive coupled contactless energy transfer systems – a review," in: Proc. WZEE, 1–6 (2015).
[3] X. Wei, Z. Wang, and H. Dai, "A Review of Wireless Power Transfer via Strongly Coupled Magnetic Resonances", *Energies*, 7, 4316–4341 (2014).
[4] Y. Zhaksylyk and M. Azadmehr, "Comparative Analysis of Inductive and Capacitive Feeding of Magnetic Resonance Wireless Power Transfer," in: *2018 IEEE PELS Workshop on Emerging Technologies: Wireless Power Transfer (Wow)*, 1–5 (2018).
[5] J. Hu and C.K. Lee, "Distance and Misalignment Adaption Analysis of Inductive and Radio Frequency Power Transmission," in: *2018 IEEE PELS Workshop on Emerging Technologies: Wireless Power Transfer (Wow)*, 1–5 (2018).
[6] G. Blakiewicz, J. Jakusz, W. Jendernalik, and S. Szczepański, "Automatic tuning of a resonant circuit in wireless power supply systems for biomedical sensor," *Bull. Pol. Ac.: Tech.*, 64(3) 641–646 (2016).
[7] M. Manoufali, K. Bialkowski, B. Mohammed, and A. Abbosh, "Wireless Power Link Based on Inductive Coupling for Brain Implantable Medical Devices," *IEEE Antennas Wirel. Propag. Lett.*, 17(1), 160–163 (2018).
[8] M. Schormans, V. Valente and A. Demosthenous, "Practical Inductive Link Design for Biomedical Wireless Power Transfer: A Tutorial," *IEEE Transactions on Biomedical Circuits and Systems*, 12(5), 1112–1130 (2018).
[9] A. Ahmad, M.S. Alam, and R. Chabaan, "A Comprehensive Review of Wireless Charging Technologies for Electric Vehicles," *IEEE Transactions on Transportation Electrification*, 4(1), 38–63 (2018).).
[10] C. Auvigne, P. Germano, D. Ladas, and Y. A. Perriard, "A dual-topology ICPT applied to an electric vehicle battery charger", in: *2012 XXth Int. Conf. Electr. Mach.* 2287–2292 (2012). doi:10.1109/ICElMach.2012.6350201.

[11] R. Bosshard, J.W. Kolar, J. Mühlethaler, I. Stevanovic, B. Wunsch, and F. Canales, "Modeling and η-α-Pareto optimization of inductive power transfer coils for electric vehicles," *IEEE J. Emerg. Sel. Topics Power Electron.*, vol. 3, no. 1, pp. 50–64, Mar. 2015.

[12] Z. Huang, S.-C. Wong, and Chi K. Tse, "An Inductive Power Transfer Converter With High Efficiency Throughout Battery Charging Process," *IEEE Transactions on Power Electronics*, 34 (X), 2019; DOI 10.1109/TPEL.2019.2891754.

[13] S. Judek and K. Karwowski, "Supply of electric vehicles via magnetically coupled air coils", in: *2008 13th Int. Power Electron. Motion Control Conf. EPE-PEMC 2008* 1497–1504 (2008). doi:10.1109/EPEPEMC.2008.4635479.

[14] M. Kesler, "Wireless Charging of Electric Vehicles," in: *2018 IEEE Wireless Power Transfer Conference (WPTC)*, 1–4 (2018).

[15] M. Kim and B. K. Lee, "System Design and Control of Inductive Power Transfer for Electric Vehicles Considering Wide Variation of Output Voltage and Coupling Coefficient", *IEEE Transactions on* Power *Electronics*, 34(2) 1197–1208 (2019)

[16] Y. Lu, F. Mao, and R. P. Martins, "Bi-directional Battery-to-Battery Wireless Charging Enabled by Reconfigurable Wireless Power Transceivers (Invited Paper)", in: *2018 IEEE International Conference on Electron Devices and Solid State Circuits (EDSSC)*, 1–2 (2018).

[17] P. Machura and Q. Li, "A Critical Review of Wireless Charging for Electric Vehicles". *Renewable and Sustainable Energy Reviews*, Elsevier, 104(4), 209–234 (2019)

[18] A.J. Moradewicz and M.P. Kazmierkowski, High efficiency contact-less energy transfer system with power electronic resonant converter", *Bull. Pol. Ac.: Tech.*, 57(4) 375–381 (2009)

[19] M.J. Neath, A.K. Swain, U.K. Madawala, D.J. Thrimawithana, and D.M. Vilathgamuwa, "Inductive Power Interface for Electric Vehicles Controller Synthesis of a Bidirectional", in: *2012 IEEE Third International Conference on Sustainable Energy Technolog. (ICSET)* 60–65 (2012). doi:10.1109/ICSET.2012.6357376.

[20] C. Panchal, S. Stegen, and J. Lu, "Review of static and dynamic wireless electric vehicle charging system", *Engineering Science and Technology, an International Journal* (21) 922–937 (2018).

[21] D. Patil, M.K. McDonough, J.M. Miller, B. Fahimi, and P.T. Balsara, "Wireless Power Transfer for Vehicular Applications: Overview and Challenges", *IEEE Transactions on Transportation Electrification* , 4(1) 3–37 (2018).

[22] J. Kim, B. Lee, J. Lee, S. Lee, C. Park, S. Jung, S. Lee, K. Yi, and J. Baek, "Development of 1MW inductive powert Transfer system for a high speed train, "*IEEE Tranactions on Industrial Electron*ics 62(10) 6242–6250 (2015).

[23] R.M. Miskiewicz, "Contactless Supply Systems with Bidirectional Energy Flow", PhD Thesis, Electrotechnical Institute Warsaw, 2016

[24] L. Zhao, D.J. Thrimawithana, and U.K. Madawala, "A hybrid bi-directional IPT system with improved spatial tolerance", in: *2015 IEEE 2nd International Future Energy Electronics Conference, IFEEC 2015*, 1–6 (2015). doi:10.1109/IFEEC.2015.7361591.

[25] R. Bosshard, J.W. Kolar, and B. Wunsch, "Control method for Inductive Power Transfer with high partial-load efficiency and resonance tracking", in: *2014 International Power Electronics Conference, IPEC-Hiroshima – ECCE Asia 2014* 2167–2174 (IEEE, 2014). doi:10.1109/IPEC.2014.6869889.

[26] B. Minnaert and N. Stevens, "Maximizing the Power Transfer for a Mixed Inductive and Capacitive Wireless Power Transfer System", in: *2018 IEEE Wireless Power Transfer Conference (WPTC)*, 1–4 (2018).

[27] M. Lu and K.D.T. Ngo, "Systematic Design of Coils in Series–Series Inductive Power Transfer for Power Transferability and Efficiency", *IEEE Transactions on Power Electronics*, 33(4), 3333–3345 (2018).

[28] M. Marcinek, H. Hołub, S. Kalisiak, and R. Pałka "Resonant frequency stabilization technigue in series-series contactless energy transfer systems", *Archives of electrical engineering*, 66(3) 547–558 (2017).

[29] A. Sharma and D. Kathuria, "Performance Analysis of a Wireless Power Transfer System based on Inductive Coupling", in: *2018 International Conference on Computing, Power and Communication Technologies (GUCON)*, 55–59 (2018).

[30] D. Vincent, S. Chakraborty, P.S. Huynh, and S.S. Williamson, "Efficiency analysis of a 7.7 kW inductive wireless power transfer system with parallel displacement", in: *2018 IEEE International Conference on Industrial Electronics for Sustainable Energy Systems (IESES)*, 409–414 (2018).

[31] Z. Huang, S.-C. Wong and C.K. Tse, "Control Design for Optimizing Efficiency in Inductive Power Transfer Systems", *IEEE Transactions on* Power *Electronics*, 33(5), 4523–4534 (2018)

[32] J.T. Matysik, "The current and volatge phase shift regulation in resonant converter with integration control", *IEEE Trans. Ind. Electron.* 54, 1240–1242 (2007).

[33] P.C. Ghosh, P.K. Sadhu, and A. Ghosh "A new circuit topology using Z-source resonant inverter for high power contactless power transfer application", *Archives of electrical engineering*, 66(4), 843–854 (2017).

[34] T. Diekhans and R.W. De Doncker, "A Dual-Side Controlled Inductive Power Transfer System Optimized for Large Coupling Factor Variations and Partial Load", *IEEE Trans. Power Electron.* 30, 6320–6328 (2015).

[35] S. Jeschke, M. Maarleveld, J. Baerenfaenger, B. Schmuelling, and A. Burkert, "Challenges in EMC Testing of EV and EVSE Equipment for Inductive Charging", in: *2018 International Symposium on Electromagnetic Compatibility (EMC EUROPE)*, 967–971 (2018).

[36] H. Kim, C. Song, J. Kim, D.H. Jung, E. Song, S. Kim, and J. Kim, "Design of magnetic shielding for reduction of magnetic near field from wireless power transfer system for electric vehicle", in 2014 International Symposium on Electromagnetic Compatibility, Sept 2014.

[37] M. Mohammad, E.T. Wodajo, S. Choi, and M. Elbuluk, "Modeling and Design of Passive Shield to Limit EMF Emission and to Minimize Shield Loss in Unipolar Wireless Charging System for EV", *IEEE Transactions on Power Electronics*, 34(X), 2019; DOI 10.1109/TPEL.2019.2903788.

[38] *IEEE Standard for Safety Levels With Respect to Human Exposure to Radio Frequency Electromagnetic Fields, 3 kHz to 300 GHz*, Standard C95.1–2005, Apr. 2006.

[39] International Commission on Non-Ionizing Radiation Protection (ICNIRP), "Guidelines for limiting exposure to time-varying electric and magnetic fields (1 Hz to 100 kHz)", *Health Phys.*, vol. 99 (6), 818–836 (2010), also avialable on: https://www.icnirp.org/cms/upload/publications/ICNIRPLFgdl.pdf

[40] *Wireless Power Transfer for Light-Duty Plug-In/Electric Vehicles and Alignment Methodology*, Standard SAEJ2954, Available: http://standards.sae.org/j2954_201605/

[41] Electric Vehicle Wireless Power Transfer (WPT) Systems–Part I: General *Requirements, Engineering 360*, Standard IEC 61980–1; http://standards.globalspec.com/std/10072168/iec-61980–1